Applied Surface Science 428 (2018) 739–747

Contents lists available at ScienceDirect

Applied Surface Science

journal homepage: www.elsevier.com/locate/apsusc

Full Length Article

# Synthesis of barbituric acid doped carbon nitride for efficient solar-driven photocatalytic degradation of aniline

Lin Li[a], Qingguo Meng[b], Haiqin Lv[b], Lingling Shui[a], Yongguang Zhang[c], Zhang Zhang[c,d], Zhihong Chen[b,c,*], Mingzhe Yuan[b], Richard Nötzel[a,c], Xin Wang[a,c,*], Jun-Ming Liu[d,e], Guofu Zhou[a]

[a] Institute of Electronic Paper Displays, South China Academy of Advanced Optoelectronics, South China Normal University, Guangzhou, Guangdong Province, China
[b] Shenyang Institute of Automation, Guangzhou, Chinese Academy of Sciences, Guangzhou 511458, China
[c] International Academy of Optoelectronics at Zhaoqing, South China Normal University, Guangdong Province, China
[d] Institute of Advanced Materials, South China Academy of Advanced Optoelectronics, South China Normal University, Guangzhou, Guangdong Province, China
[e] Laboratory of Solid State Microstructures, Nanjing University, Nanjing 210093, China

ARTICLE INFO

*Article history:*
Received 11 July 2017
Received in revised form
12 September 2017
Accepted 19 September 2017
Available online 20 September 2017

*Keywords:*
Carbon nitride
Copolymerizing
Barbituric acid
Photodegradation
Aniline

ABSTRACT

A series of barbituric acid doped carbon nitride (CN-BA) photocatalysts were successfully prepared by copolymerizing dicyandiamide with barbituric acid (BA). Under AM1.5 simulated sunlight, CN-BA photocatalysts exhibit enhanced photocatalytic activity compared to pure carbon nitride for the degradation of aniline. The highest activity is obtained with 2% doped CN-BA photocatalyst.
*Results:* on the photodegradation of aniline indicate that for the optimized CN-BA photocatalyst, the concentration of aniline solution was reduced gradually from 16 mg/L to 1.354 mg/L in 2 h. This corresponds to a 6 times higher photodegradation efficiency than pure carbon nitride samples. The enhanced photocatalytic activity of CN-BA relies on the enhanced surface area, the higher light absorption and the reduced recombination of the photo-generated electron-hole pairs. This interpretation results from multiple characterizations with EPR, BET, $N_2$ adsorption, Solid-state $^{13}C$ NMR, UV–vis DRS, FESEM, and TEM. Under simulated sunlight irradiation, CN-BA is excited and generates electron-hole pairs. The photogenerated electrons in the CN-BA conduction band react with the molecular oxygen to form $^{\bullet}O_2^-$. Part of the $^{\bullet}O_2^-$ transforms into $^{\bullet}OH$, which further oxides aniline. Meanwhile, photo-generated holes in the valence band of CN-BA can benefit to the formation of $^{\bullet}OH$ or directly oxide aniline.


## 1. Introduction

Aniline is an important precursor and intermediate compound which has been widely applied in the industrial production of polyurethanes, pharmaceuticals, pesticides and rubber additives [1,2]. However, aniline is a highly toxic and cancer-causing compound which is now considered as a major environmental pollutant. Nowadays, the major treatment processes for industrial aniline wastewater are based on bio-degradation and physical-adsorption methods [3]. But the aniline bio-degradation efficiency is quite low because of its high biological-toxicity. Physical-absorption method is costly and unsuitable for degrading low-concentration industrial aniline wastewater. Therefore, it is critical to look for a low-cost, high-efficient and environmental friendly method for treating industrial aniline wastewater.

In recent years, semiconductor-based photocatalytic degradation has been regarded as a low cost, efficient and environmental friendly strategy to treat wastewater containing aniline [4–8]. $TiO_2$ have been widely used as a photocatalysts for the photocatalytic degradation of aniline in an aqueous solution under visible light irradiation. However, $TiO_2$ can only respond to UV irradiation, so there is a weak visible-light response when using $TiO_2$-based photocatalysts which strongly limits its practical applications under

* Corresponding author at:Institute of Electronic Paper Displays, South China Academy of Advanced optoelectronics, South China Normal University, Guangzhou, Guangdong Province, China; Shenyang Institute of Automation, Guangzhou, Chinses Academy of Sciences, Guangzhou, China; International Academy of Optoelectronics at Zhaoqing, South China Academy of Advanced optoelectronics, South China Normal University, Guangdong Province, China.
*E-mail addresses:* chenzhihong1227@sina.com (Z. Chen), wangxin@scnu.edu.cn (X. Wang).

http://dx.doi.org/10.1016/j.apsusc.2017.09.161
0169-4332/

solar light. Therefore, developing novel high visible-light-response photocatalysts with high-efficiency and stability has become a hot topic in the field of the photocatalytic degradation of aniline.

Recently, a polymeric semiconductor photocatalyst, graphitic carbon nitride (CN), has attracted a great attention because of its relative narrow band gap, sufficiently negative conduction-band position and high chemical stability [9]. However, the photocatalytic activity of CN versus the degradation organic pollutants is quite low because of its relatively fast charge recombination and insufficient absorption in the visible-light spectral range. To improve the photocatalytic performance of CN, various modification methods have been applied through structure regulation [10–19], doping [20–27], surface hetero-junction and copolymerization [28–37]. Among those methods, copolymerization of CN has been regarded as an efficient route, not only for obtaining an enhance light-absorption, but also for creating surface hetero-structures which could reduce the recombination of photogenerated electron-holes.

In this study, barbituric acid doped graphitic carbon nitride (CN-BA) photocatalysts were synthesized by copolymerizing dicyandiamide (DCDA) with barbituric acid (BA) to improve the optical absorption, electronic and photoelectric properties of carbon nitride. Moreover, the catalytic activity of CN-BA versus the degradation of aniline in aqueous solution was investigated for the first time. All as-prepared CN-BA samples exhibited a higher photocatalytic degradation of aniline in aqueous solution respect to pure CN and the CN-BA-2.0 sample (see details in the experimental section) resulted in the highest photocatalytic activity. The concentration of aniline in aqueous solution degraded from 16 to 1.354 mg/L in the presence of CN-BA-2.0 under simulated sunlight irradiation for 2 h. The structure, surface area and optical properties of CN-BA samples were characterized by XRD, SEM, TEM, XPS, DRS and EPR spectra. The combined benefits of the BA doping in terms of optical, surface and texture properties lead to a significant improvement in the photocatalytic activity for degradation of aniline in aqueous solution under simulated sunlight irradiation. The mechanism leading to the photocatalytic degradation of aniline was also investigated systemically.

## 2. Experimatal methods

### 2.1. Chemicals

All chemical reagents were of analytical grade. Dicyandiamide and barbituric acid (BA) were purchased from Sigma-Aldrich Química. Deionized water was used throughout in photocatalytic experiments.

### 2.2. Synthesis of CN and CN-BA

For the synthesis of CN samples, 2.0 g of dicyandiamide were sealed in a quartz boat and heated in air to 550 °C for 4 h with a heating-rate of 2.3 °C/min [38].

The BA doped CN samples were synthesized from dicyandiamide and BA by a thermal polymerization process. In a typical process, 2.0 g of dicyandiamide and different quality of BA were dispersed in 20 mL of deionized water. Water was successively removed by heating at 100 °Cunder stirring. The dried solid was grinded, transferred into a quartz boat and be calcined in air at 550 °C for 4 h at the heating-rate of 2.3 °C/min. Resulting samples were denoted as CN-BA-X, where X (0.2, 0.5, 1.0, 2.0, 3.0) represents the mass fraction of BA.

### 2.3. Characterization

Crystallographic phases of powder were analyzed by X-ray diffraction (XRD) from X'Pert PRO. Fourier transformed infrared (FTIR) spectra were acquired with a Nicolet Magna-IR 170 spectrometer. The solid-state [13]C NMR spectra were recorded using a Bruker Advance III 500 spectrometer. X-ray photoelectron spectroscopy (XPS) measurements were performed on Thermo ESCALAB 250Xi instrument with a monochromatized Al Ka line source (150 W). Electron paramagnetic resonance (EPR) measurements were performed on a Bruker ER200-SRC spectrometer. The UV–vis diffuse reflectance spectra (UV–vis DRS) were recorded on a U-41000, HITACHI spectrophotometer, Tokyo, Japan by using $BaSO_4$ as a reflecting sample. Surface morphology and structure were examined by ZEISS Ultra 55 field-emission scanning electron microscope (FESEM). Transmission electron microscopy (TEM) images were collected by using a JEM-2100HR field emission electron microscope. The Brunauer–Emmett–Teller (BET) surface area was determined with a Quantachrome Instruments Quadrasorb SI.

### 2.4. Photocatalytic test for degradation of aniline

The concentration of aniline in the aqueous solution was measured using a colorimetric method. In a typical experiment, the photocatalytic degradation of aniline was measured using a 300 W Xe lamp (AM 1.5, output light current is 15 A) as simulated sunlight. 100 mg of the as-prepared photocatalyst were added into 150 mL of an aqueous solution containing an aniline concentration of 16 mg/L. The suspension was stirred for 30 min with light irradiation to reach the absorption-desorption equilibrium. Then simulated sunlight irradiation was activated by shining the suspension with a 300W Xe lamp (output light intensity is 1 sun, AM 1.5, 100 mW/cm$^2$). At time intervals of 30 min, the solution was sampled and centrifuged to remove the catalysts. The concentration of aniline within the centrifuged solution was determined by a colorimetric method. The detection limit method was estimated to be 1.6 mg/L.

### 2.5. The colorimetric method

The $KHSO_4$ (50 g/L), $NaNO_2$ (50 g/L), $NH_3SO_3NH_2$ (25 g/L) and N-(1-Naphthyl) ethylenediaminedi hydrochloride (20 g/L) solutions were prepared in 50 mL conical flasks, respectively. 1 mL of the photodegraded (centrifuged) solution and 9 mL of deionized water were introduced into the 25 mL test tube with a glass stopper, then 1 mL of $KHSO_4$ solution was added to the solution. After that, a drop of $NaNO_2$ solution was introduced into the solution. Finally the $NH_3SO_3NH_2$ solution was used to wipe out the $NaNO_2$ excess by adding into the above mixture until a uniform solution was formed. After bubbles were entirely wiped out, 1 mL of N-(1-Naphthyl) ethylenediamine dihydrochloride chromogenic agent was added and the solution was diluted to 25 mL with deionized water. The absorbance of the aniline solution was then detected by 1 cm cell at 545 nm on a UV–vis spectroscopy after 30 min.

### 2.6. Photo-electrochemical experiments

To prepare the working electrodes, 300 mg of the sample and 20 mg 2-Naphthol

were grinded and dispersed in ethanol to form a slurry. Then the slurry was coated on FTO conductive glass sheet. After drying at 120 °C for 2 h in vacuum, the working electrodes were obtained. Photocurrent measurements were carried out in a conventional three-electrode electrochemical workstation (CHI 660E). Pt sheet and Ag/AgCl electrode were used as the counter and reference electrodes, respectively. A 0.5 M $Na_2SO_4$ aqueous solution served as

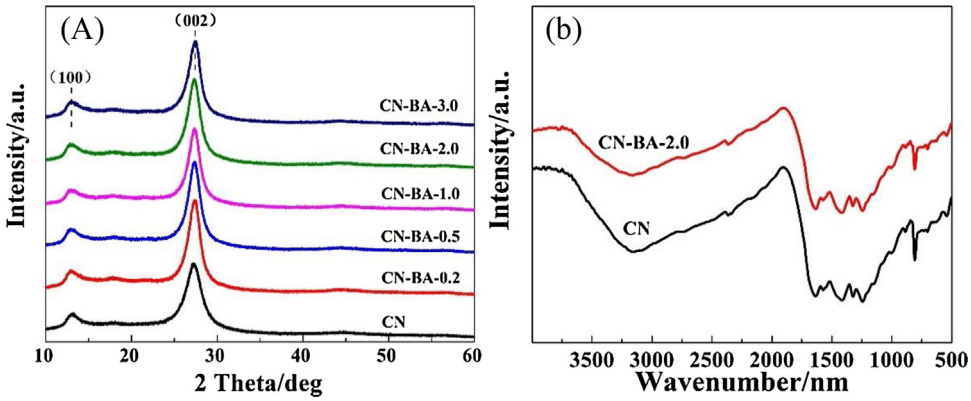


**Fig. 1.** XRD (A) patterns of the samples of CN and CN-BA-X, and FTIR spectra (B) of the samples of CN and CN-BA-2.0.

the electrolyte. The irradiated area of the working electrode was 1 $cm^2$. The intensity of the incident light was 100 $mW/cm^2$ (AM 1.5 G, 300-W xenon lamp). The 320 s period on-and-off photocurrent responses of CN and CN-BA-2.0 samples were obtained at 0 V bias vs Ag/AgCl.

## 3. Results and discussion

### 3.1. XRD and FTIR characterization

XRD analysis was applied to check the crystal phase of CN and CN-BA samples. As shown in Fig. 1A, XRD patterns of pure CN and BA-doped CN samples show distinct diffraction peaks at 13.0° and 27.3°, suggesting that the BA doping does not change the CN phase structure. The diffraction peak at 13.0° was indexed to the (100) plane, corresponding to the interlayer structural of CN sheets. The diffraction peak at 27.3° was indexed to (002) plane, the graphite-like material.

FTIR spectra (Fig. 1B) were recorded for CN and CN-BA-2.0 samples. The similar stretch peaks were observed, suggesting that the BA doping does not alter the core chemical skeleton integrality of CN. Typical stretch modes of aromatic CN heterocycles in the region of 1200–1600 $cm^{-1}$ and breathing mode of the heptazine units ($C_6N_7$) at 810 $cm^{-1}$ were observed in both CN and CN-BA-2.0 samples, confirming the presence of a triazine phase. In addition, we could observe that broad bands appear in the range of 2900–3700 $cm^{-1}$ due to the N—H vibration and $H_2O$ molecules.

### 3.2. XPS characterization

XPS measurements were conducted to get insights into the chemical composition and chemical state of the elements in the BA-doped CN samples. As shown in Fig. 2A, the survey spectra of CN-BA-2.0 and CN indicate the presence of C, N and O elements without other contaminants, which confirms that the elemental composition corresponds to CN-BA-2.0 and CN samples. Fig. 2 B shows the high-resolution C1 s spectra of CN-BA-2.0 and CN samples. Two peaks were observed for the CN sample at 285.1 eV and 288.6 eV, corresponding to C—N—C and C—$(N)_3$, respectively. Compared to the CN sample, the two peaks for CN-BA-2.0 were slightly shifted and located at 285.2 eV and 288.5 eV, respectively [39]. This slight shift in the peaks of CN-BA-2.0 is probably due to introduction of BA into the framework of CN, which changes its binding energy. Fig. 2C presents the high-resolution N1 s spectra of CN-BA-2.0 and CN samples. Four peaks of the CN sample can be distinguished at 398.9 eV, 399.8 eV, 401.1 eV and 404.6 eV. The stronger peak at 398.9 eV was assigned to the ring nitrogen in the sp2 C—N=C bonds. The weak peak at 399.8 eV indicated the presence of tertiary nitrogen $N(C)_3$ groups. In addition, the peak at 401.1 eV was attributed to the presence of amino groups (CNH) and the peak at 404.6 eV was assigned to the charge effects or the positive charge localization in heterocycles [40]. Additionally, the peaks for C—N=C bonds and $N(C)_3$ groups of CN-BA-2.0 sample were also slightly shifted, likely due to the formation of tri-s-triazine based covalent networks through BA doped CN [41]. Fig. 2D presents the high-resolution O1 s XPS spectra of CN-BA-2.0 and CN samples. A single peak was observed at 532.2 eV, which is in agreement with the CN-BA-2.0 and CN composition. This peak was due to the $H_2O$ groups adsorbed on the CN-BA-2.0 surface. A gradual increase in the C/N molar ratio from 0.805 for pristine CN to 0.814 for CN-BA-2.0 reveals the successful integration of BA rings into the CN network.

### 3.3. Solid-state $^{13}C$ NMR characterization

Solid-state $^{13}C$ NMR spectroscopy was used to further characterize the BA-doped CN, as shown in Fig. 3. The spectrum clearly shows the appearance of a new broad peak at 97.9 ppm for the CN-BA-2.0 sample, which indicates that BA was doped in the CN-conjugated network but the heptazinc-based structure of CN did not change [42,43].

### 3.4. EPR characterization

EPR measurements were performed to investigate the electronic band structure of CN and BA-doped CN samples. Samples in dark or visible light irradiation show the presence of only one single Lorentzian line centered at 3146.3 G with a g-value of 2.0034 (Fig. 4). This suggests the presence of well-defined semiconductor properties. The EPR signal intensity of CN-BA-2.0 is 1354, which is about 6 times higher than in CN (212). It was previously demonstrated that the efficient generation of photochemical radical pairs is highly beneficial in photocatalytic degradation reactions. Interestingly, an enhanced EPR signal was observed when CN and CN-BA were irradiated with visible light, indicating an efficient photochemical generation of radical pairs within the semiconductors.

### 3.5. $N_2$ adsorption–desorption isotherms characterization

$N_2$ adsorption-desorption measurements were carried to investigate textual properties of CN and CN-BA-2.0 samples. As show in Fig. 5, samples exhibit a similar IV behavior with a H1 type hysteresis loop. In additional, the inset indicates that the BET surface area of CN-BA-2.0 (16.251 $m^2/g$) is higher than in CN (10.469 $m^2/g$). However, the pore size of CN-BA-2.0 (4.450 nm) was comparable with the undoped CN (4.458 nm). This suggests that the BET surface area and the pore size of pure CN were amplified and decreased,

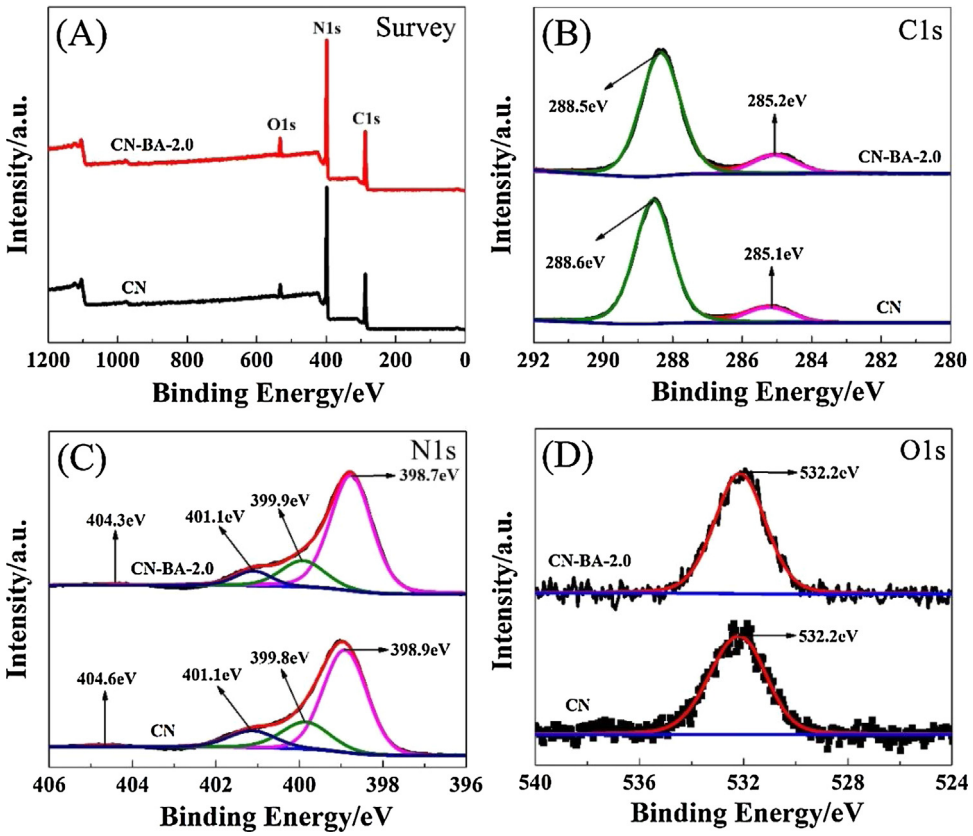


**Fig. 2.** High-resolution XPS spectra of the as prepared CN-BA-2.0 and CN samples: The survey spectra (A), C1 s (B), N1 s (C) and O1 s (D) spectra of the CN-BA-2.0 and CN samples.

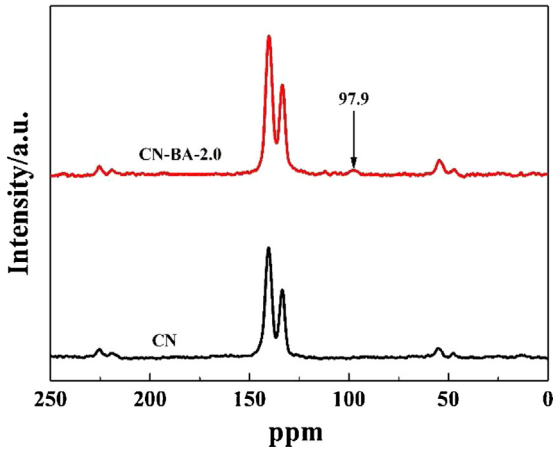


**Fig. 3.** Solid-state 13C NMR spectra for CN and CN-BA-2.0 samples.

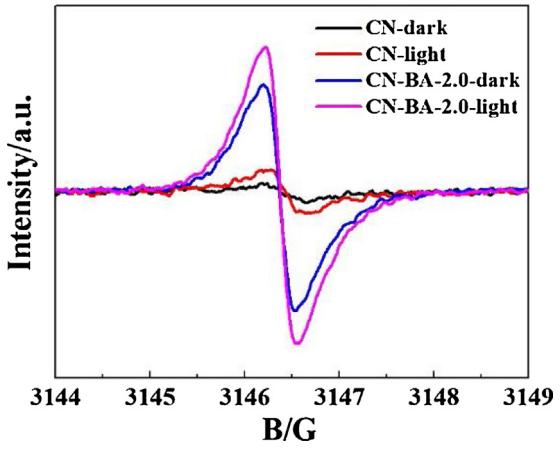


**Fig. 4.** EPR spectra in the dark and under visible light (λ > 420 nm) for CN and CN-BA-2.0 samples.

respectively upon doping. These structural modifications remarkably improved the photocatalytic activity respect to pure CN.

### 3.6. UV–vis DRS characterization

UV–vis DRS spectra of CN and CN-BA-X samples are shown in Fig. 6. Interestingly, CN-BA samples show a higher light-absorption in the visible range respect to pure CN. This corresponds to a change of the powder color from bright yellow to deep orange (see inset in Fig. 6), suggesting that BA doping induced modifications could enhance the light-absorption in visible light region.

### 3.7. SEM and TEM characterization

TEM and SEM analyses were applied to study the morphology and the microstructure of CN and CN-BA-2.0 samples. As shown in Fig. 7A, the SEM image of CN clearly show dense clumps and stacked massive particles, while the image of CN-BA-2.0 (Fig. 7B) shows that the sample is constituted of a looser lamellar structure, resulting in the enlarged surface area. Moreover, it can be clearly seen from TEM images of CN (Fig. 7C) and CN-BA-2.0 (Fig. 7D) that dense stacks in CN skeleton transform into much thinner sheets structures after BA doping.

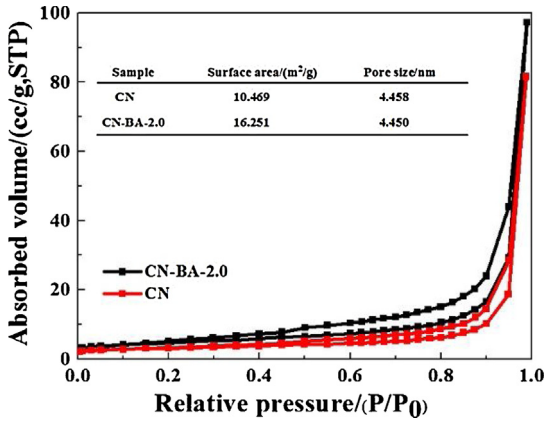


**Fig. 5.** $N_2$ adsorption-desorption isotherms of CN and CN-BA-2.0, the inset shows the surface and pore size of CN and CN-BA-2.0 samples.

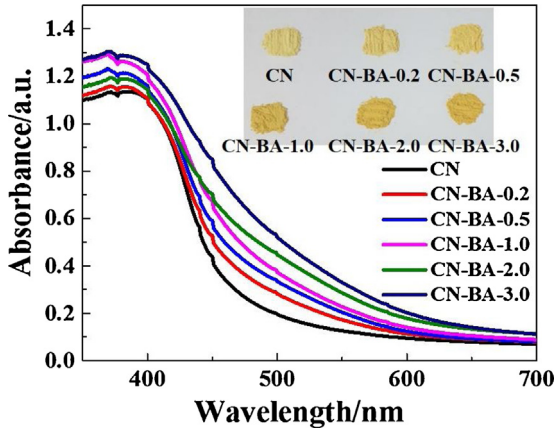


**Fig. 6.** UV–vis DRS spectra of the samples of CN and CN-BA-X, the inset is the optical picture of as-prepared CN-BA-X samples.

### 3.8. Photocatalytic activity and stability of CN and CN doped of BA

The photocatalytic properties of CN and CN-BA samples were evaluated by studying the degradation of aniline in aqueous solution under simulated sunlight irradiation. Experimental results are reported in Fig. 8. As shown in Fig. 8A, BA-doped CN samples showed a higher photocatalytic activity respect to CN; this may be resulted from the enhanced surface area and optical absorbance and the reduction of the recombination of photo-generated electron-hole pairs. Meanwhile, the CN-BA-2.0 shows the highest photocatalytic activity for the degradation of aniline. As the mass fraction of BA was increased over 2.0, a decrease in the photocatalytic activity of CN-BA was observed. The probable reason for this is that a too high BA doping could lead to higher recombination of photo-generated electron-hole pairs, which cancels the beneficial effect due to the higher surface area and wider optical absorbance. Fig. 8 B shows temporal absorbance spectra and optical chromogenic images of aqueous aniline which give a direct estimation of the aniline concentration within the solution. The typical absorption peak of the chromogenic aniline aqueous solution at 545 nm gradually decreases with the simulated sunlight irradiation time; this is associated with a gradual color change of the solution from dark purple to transparent.

To further investigate the photocatalytic reaction of degradation of aniline, the reaction kinetics of degradation of aniline was conducted, and the kinetic equation of aniline degradation shows a first-order kinetic model (Eq. (1)) according to the kinetic linear curves.

$$R = \frac{dC}{dt} = \frac{kKC}{1+KC} \quad (1)$$

Where $R$ is the degradation rate of the reactant ($mg \bullet L^{-1} \bullet min^{-1}$), $C$ and $t$ represent the concentration of the reactant ($mg \bullet L^{-1}$) and the irradiation time, respectively. Meanwhile,$k$ and $K$ represent the reaction rate constant ($mg \bullet L^{-1} \bullet min^{-1}$) and the adsorption coefficient of reactant ($L \bullet mg^{-1}$). While the Eq. (1) was changed the first-order kinetic model through simplified when the initial concentration ($C_0$) was very low. Specific as follow:

$$\ln \frac{C_0}{C} = kKt = K_{app}t \quad (2)$$

Where $K_{app}$ is the apparent first-order rate constant ($min^{-1}$). As shown in Fig. 9A and 9B, the apparent first-order rate constant order of BA doped CN samples was CN-BA-2.0 > CN-BA-3.0 > CN-BA-1.0 > CN-BA-0.5 > CN-BA-0.2 > CN. It was found that CN-BA-2.0 shows the highest apparent first-order rate constant (0.02189 $min^{-1}$), which is about 6 times higher than that of pristine CN (0.00293 $min^{-1}$).

Photo-electrochemical experiments were performed to investigate the ability of the as-prepared samples for photoinduced charge carriers generation and separation. It can be seen from Fig. 10A that pure CN exhibits lower photocurrent intensity than CN-BA-2.0 sample, indicating that there was efficient photoinduced charge generation after BA was doped into pure CN. Additionally, the higher photocurrent intensity indicates better separation efficiency of electrons and holes [44]. Therefore, the result clearly revealed that BA doped in CN framework can significantly enhance the separation of photo-generated electron-hole pair.

It is very important to evaluate the stability of photocatalysts for practical applications. Therefore, we carried out repeated photocatalytic experiments with CN-BA-2.0 for aniline degradation under the same conditions. As shown Fig. 10B, the photocatalytic activity of CN-BA-2.0 sample is slightly deactivated after five successive cycles of photodegradation of aniline, which indicates that the photocatalyst has good stability under simulated sunlight irradiation.

### 3.9. Free radical and hole scavenging experiments

In the photocatalytic oxygen process, a series of reactive oxygen species, such as $^{\bullet}OH$, $^{\bullet}O_2^-$, $h^+$ or $H_2O_2$ were supposed to be involved. To distinguish the reactive oxy-radical, the trapping experiments and reactive radical qualitative detection were conducted. In the trapping experiment, isopropanol (IPA), $N_2$ and ammonium oxalate (AO) were served as the hydroxyl radical ($^{\bullet}OH$) scavenger, superoxide radical ($^{\bullet}O_2^-$) scavenger and hole ($h^+$) scavenger, respectively [45]. It can be seen (Fig. 11A) that the addition of IPA, $N_2$ and AO in the aniline solution has strong adverse effect on the photocatalytic activity of CN-BA samples, suggesting that $^{\bullet}OH$, $^{\bullet}O_2^-$ and $h^+$ may be the main oxygen species in the photocatalytic oxygen process. The strongest hindering effect on the photocatalytic activity in those oxygen species is $^{\bullet}O_2^- > {}^{\bullet}OH > h^+$, suggesting that the $^{\bullet}OH$ was generated from the independent reaction of $^{\bullet}O_2^-$ or $h^+$. For further understanding the photocatalytic oxygen process, the radical species were detected by the EPR test, as shown in Fig. 11 B – 11D. From Fig. 11B, the results revealed that the intensity of $^{\bullet}O_2^-$ signals of the CN and CN-BA-2.0 samples increased under visible light irradiation, which is indicates that the CN and CN-BA-2.0 samples generate the $^{\bullet}O_2^-$ radicals under visible light irradiation. From Fig. 11C, it can be clearly found that the $^{\bullet}OH$ signals can only be observed in the CN-BA-2.0 testing systems under visible light irradiation. In additional, the singlet oxygen radical ($^1O_2$) signals (Fig. 11D) was found in both CN and CN-BA-2.0 testing systems under visible light irradiation, which

suggests that the $^{\bullet}O_2^-$ radicals would translated to [1]$O_2$ and $H_2O_2$ ($2^{\bullet}O_2^- + 2H^+ \rightarrow {}^1O_2 + H_2O_2$). Based on the trapping and radical qualitative experiments, some translated to $^{\bullet}OH$ and some of the $^{\bullet}O_2^-$ translated to [1]$O_2 + H_2O_2$, while the $h^+$ may transfer to $^{\bullet}OH$ or oxide the aniline directly. Therefore, according to the above discussion, the proposed photocatalytic mechanism of CN-BA was given and shown in Fig. 12. Under visible light irradiation, the CN-BA was excited and could generate electron-hole pairs. The photo-

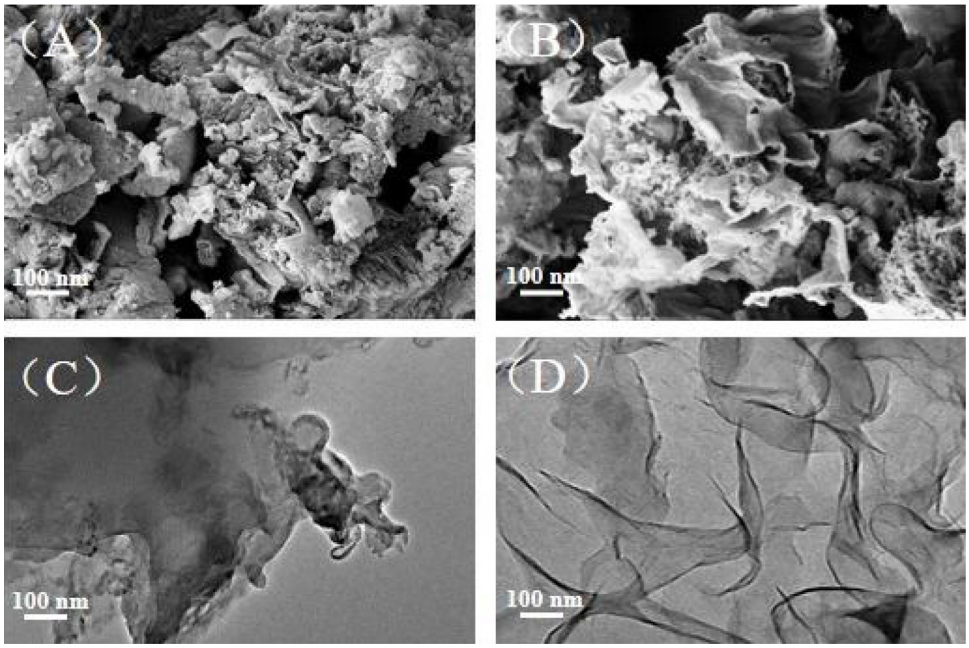


**Fig. 7.** The SEM and TEM images of the CN sample (A and C) and the CN-BA-2.0 sample (B and D).

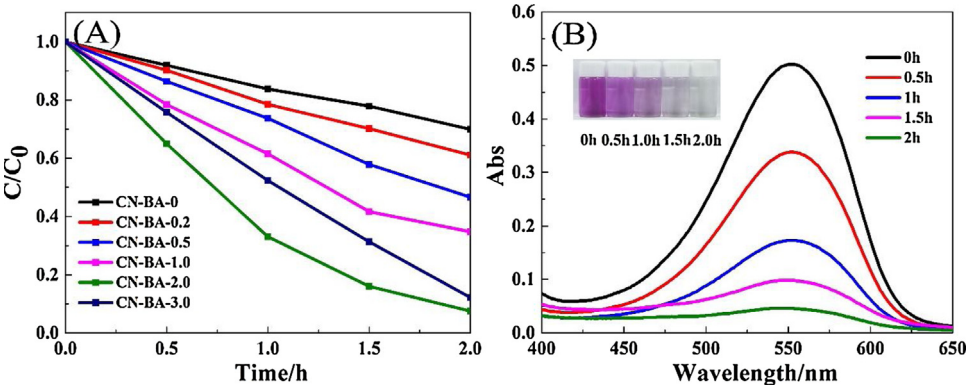


**Fig. 8.** The photocatalytic activities of the samples of CN and CN-BA-X (A) and the absorbance spectrum changes of aniline in the presence of CN-BA-2.0 (B), the inset is the color change of aniline in the presence of CN-BA-2.0.

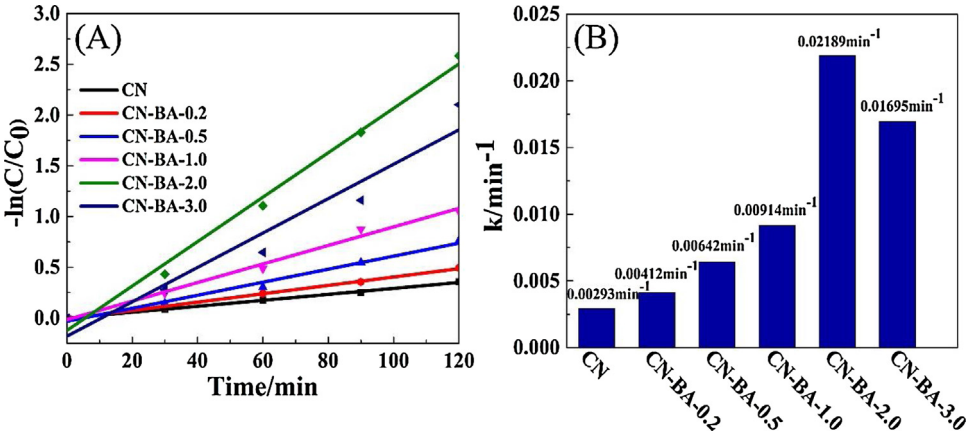


**Fig. 9.** Kinetic studies of aniline degradation (A) and the bar graph (B) of theapparent rate constants of CN and CN-BA-X.

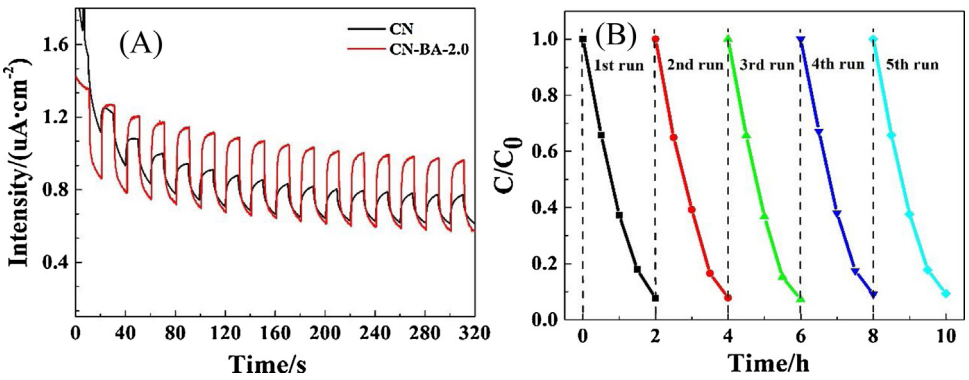


**Fig. 10.** Transient photocurrent response of CN-BA-2.0 and CN samples (A); the repeated photocatalytic experiments of CN-BA-2.0 for aniline degradation under simulated sunlight irradiation (B).

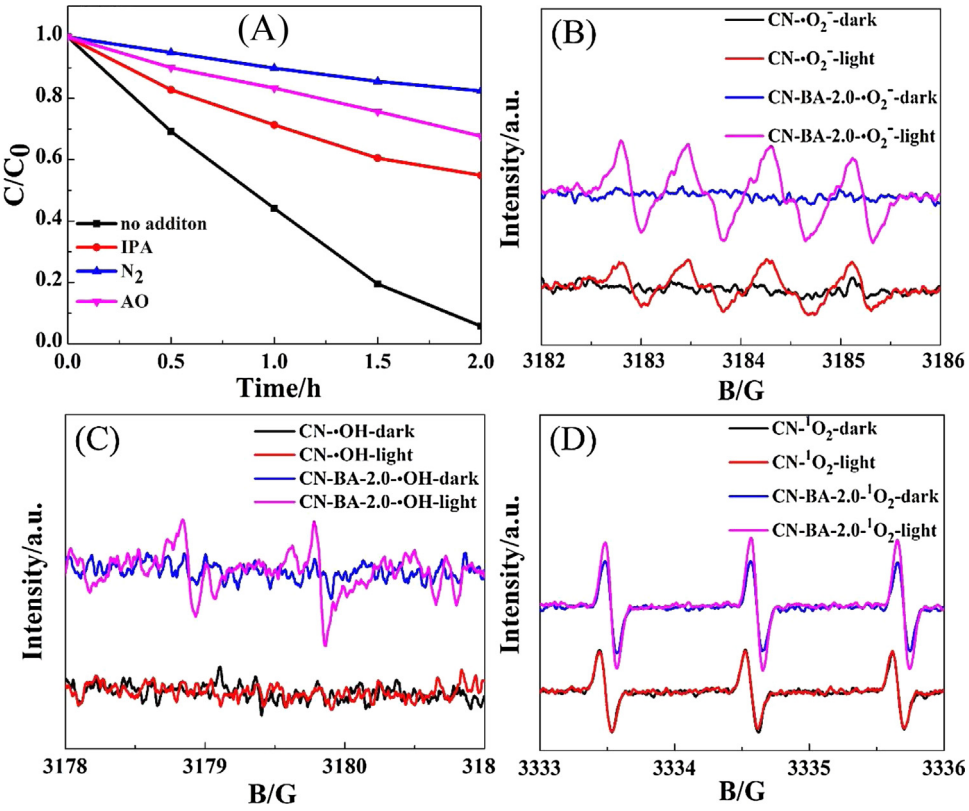


**Fig. 11.** The trapping experiment results (A) of CN-BA-2.0 and the EPR spectra of the $^{\bullet}O_2^-$ radical (B), the $^{\bullet}$OH radical (C), and the singlet oxygen radical ($^1O_2$) (D) of CN and CN-BA-2.0 samples.

generated electrons would react with the molecular oxygen to form $^{\bullet}O_2^-$ and then some of the $^{\bullet}O_2^-$ translate to $^{\bullet}$OH, which further oxide aniline. The photo-generated hole can further transfer to $^{\bullet}$OH or oxide aniline directly.

## 4. Conclusion

The BA-doped CN nanostructure photocatalysts were successfully synthesized by copolymerizing dicyandiamide with barbituric acid (BA). The BA doped CN samples exhibited the improved morphology of nanostructure, suppressed recombination of the photo-generated electron-hole pairs and high sunlight absorption. These properties make the BA-doped CN samples as a high-efficient photocatalytic material to degrade aniline. The result of degradation aniline indicated that the best sample (CN-BA-2.0) shown the dyed aniline solution changed gradually from dark purple to white after 2 h under simulated sunlight (Xe lamp) irradiation. Meanwhile, the reaction rate constant of the best sample (CN-BA-2.0) increased 6-fold for photo-degradation of aniline compared to the pure CN sample. In photocatalytic oxidation reaction process, the $^{\bullet}O_2^-$/$^{\bullet}$OOH radical plays a key role and is favorable for the photocatalytic degradation of aniline. It is ensure that we provide a simple and practical route to improve the photocatalytic activity of pure CN through CN doped BA.

## Author Contributions

L.L., ZH.C. and X.W. designed the experiments. L.L., Z.C., performed the fabrication experiments and electrochemical measurements. ZH.C. and X.W. supervised the project. L.L., QG.M., HQ.L., LL.S., YG.Z., Z.Z., ZH.C., MZ.Y., R.N., JM.L., GF.Z., and X.W. discussed the results, performed data analysis and contributed to

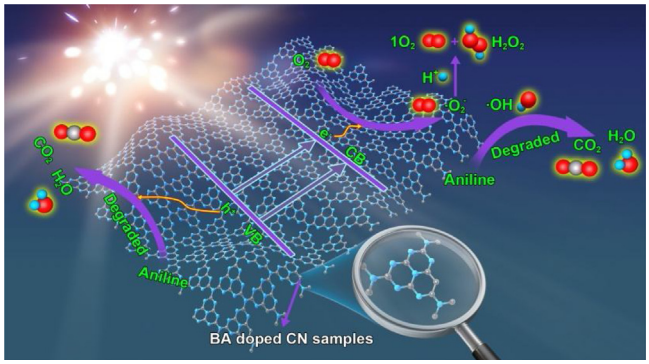


**Fig. 12.** The mechanism of the BA-doped CN samples photodegraded aniline.

manuscript writing. All the authors reviewed and commented on the manuscript.

## Acknowledgment

The authors acknowledge the financial support from the NSFC (Grant No. 51602111), the National Key R&D Program of China (2016YFB0401502), Guangdong Provincial Grant (2015A030310196, 2014B090915005), Guangdong Provincial Science and Technology Project (2017A050506009), the Pearl River S&T Nova Program of Guangzhou (201506040045), the Hundred Talent Program of Chinese Academy Sciences (QG Meng), Guangzhou Post-doctoral Initial Funding and the National 111 Project (ZH Chen), Nansha Science and Technology Project (2016GJ005).

## References

[1] H. Tang, J. Li, Y. Bie, L. Zhu, J. Zou, Photochemical removal of aniline in aqueous solutions: switching from photocatalytic degradation to photo-enhanced polymerization recovery, J. Hazard. Mater 175 (2010) 977–984.
[2] W.S. Chen, C.P. Huang, Mineralization of aniline in aqueous solution by electro-activated persulfate oxidation enhanced with ultrasound, Chem. Eng. J. 266 (2015) 279–288.
[3] J. Anotai, M.C. Lu, P. Chewpreecha, Kinetics of aniline degradation by Fenton and electro-Fenton processes, Water Res. 40 (2006) 1841–1847.
[4] L. Sánchez, J. Peral, X. Domènech, Aniline degradation by combined photocatalysis and ozonation, Appl. Catal. B-Environ. 19 (1998) 59–65.
[5] A. Kumar, N. Mathur, Photocatalytic oxidation of aniline using $Ag^+$-loaded $TiO_2$ suspensions, Appl. Catal. A-Gen. 275 (2004) 189–197.
[6] R. Hu, X. Wang, S. Dai, D. Shao, T. Hayat, A. Alsaedi, Application of graphitic carbon nitride for the removal of Pb(II) and aniline from aqueous solutions, Chem. Eng. J. 260 (2015) 469–477.
[7] W. Xiao, P. Zhou, X. Mao, D. Wang, Ultrahigh aniline-Removal capacity of hierarchically structured layered manganese oxides: trapping aniline between interlayers, J. Mater. Chem. A 3 (2015) 8676–8682.
[8] S.G. Pati, K. Shin, M. Skarpeli-Liati, J. Bolotin, S.N. Eustis, J.C. Spain, T.B. Hofstetter, Carbon and nitrogen isotope effects associated with the dioxygenation of aniline and diphenylamine, Environ. Sci. Technol. 46 (2012) 11844–11853.
[9] X. Wang, K. Maeda, A. Thomas, K. Takanabe, G. Xin, J.M. Carlsson, K. Domen, M. Antonirtti, A metal-free polymeric photocatalyst for hydrogen production from water under visible light, Nat. Mater. 8 (2009) 76–80.
[10] G. Algara-Siller, N. Severin, S.Y. Chong, T. Björkman, R.G. Palgrave, A. Laybourn, M. Antonietti, Y.Z. Khimyak, A.V. Krasheninnikov, J.P. Rabe, U. Kaiser, A.I. Cooper, A. Thomas, M.J. Bojdys, Triazine-Based, graphitic carbon nitride: a two-Dimensional semiconductor, Angew. Chem. Int. Ed. 53 (2014) 1–6.
[11] Y.S. Jun, J. Park, S.U. Lee, A. Thomas, W.H. Hong, G.D. Stucky, Three-Dimensional macroscopic assemblies of low-Dimensional carbon nitrides for enhanced hydrogen evolution, Angew. Chem. Int. Ed. 125 (2013) 11289–11293.
[12] Q. Cui, J. Xu, X. Wang, L. Li, M. Antonietti, M. Shalom, Phenyl-Modified carbon nitride quantum dots with distinct photoluminescence behavior, Angew. Chem. Int. Ed. 55 (2016) 3672–3676.
[13] D.M. Chen, J.J. Yang, H. Ding, Synthesis of nanoporous carbon nitride using calcium carbonate as templates with enhanced visible-light photocatalytic activity, Appl. Surf. Sci. 391 (2017) 384–391.
[14] H. Lan, L. Li, X. An, F. Liu, C. Chen, H. Liu, J. Qu, Microstructure of carbon nitride affecting synergetic photocatalytic activity: hydrogen bonds vs. structural defects, Appl. Catal. B-Environ. 204 (2017) 49–57.
[15] L. Lin, H. Ou, Y. Zhang, X. Wang, Tri-s-triazine-Based crystalline graphitic carbon nitrides for highly efficient hydrogen evolution photocatalysis, ACS Catal. 6 (2016) 3921–3931.
[16] M.R. Gholipour, F. Beland, T.O. Do, Post-Calcined carbon nitride nanosheets as an efficient photocatalyst for hydrogen production under visible light irradiation, ACS Sustainable Chem. Eng. 5 (2017) 213–220.
[17] Z. Zhang, Y.J. Zhang, L.H. Lu, Y.J. Si, S. Zhang, Y. Chen, K. Dai, P. Duan, L.M. Duan, J.H. Liu, Graphitic carbon nitride nanosheet for photocatalytic hydrogen production: the impact of morphology and element composition, Appl. Surf. Sci. 391 (2017) 369–375.
[18] L. Shi, L. Liang, F.X. Wang, M.S. Liu, K.L. Chen, K.N. Sun, N.Q. Zhang, J.M. Sun, Higher yield urea-derived polymeric graphitic carbon nitride with mesoporous structure and superior visible-light-responsive activity, ACS Sustainable Chem. Eng. 3 (2015) 3412–3419.
[19] Q. Gu, H.M. Sun, Z.Y. Xie, Z.W. Gao, C. Xue, $MoS_2$-coated microspheres of self-sensitized carbon nitride for efficient photocatalytic hydrogen generation under visible light irradiation, Appl. Surf. Sci. 396 (2017) 1808–1815.
[20] Z. Lin, X. Wang, Nanostructure engineering and doping of conjugated carbon nitride semiconductors for hydrogen photosynthesis, Angew. Chem. Int. Ed. 52 (2013) 1735–1738.
[21] Q.J. Fan, J.J. Liu, Y.C. Yu, S.L. Zuo, B.S. Li, A simple fabrication for sulfur doped graphitic carbon nitride porous rods with excellent photocatalytic activity degrading RhB dye, Appl. Surf. Sci. 391 (2017) 360–368.
[22] B. Chai, J.T. Yan, C.L. Wang, Z.D. Ren, Y.C. Zhu, Enhanced visible light photocatalytic degradation of Rhodamine B over phosphorus doped graphitic carbon nitride, Appl. Surf. Sci. 391 (2017) 376–383.
[23] S.S. Yi, J.M. Yan, B.R. Wulan, S.J. Li, K.H. Liu, Q. Jiang, Noble-metal-free cobalt phosphide modified carbon nitride: an efficient photocatalyst for hydrogen generation, Appl. Catal. B-Environ. 200 (2017) 477–483.
[24] S.N. Guo, Y. Zhu, Y.Y. Yan, Y.L. Min, J.C. Fan, Q.J. Xu, Holey structured graphitic carbon nitride thin sheets with edge oxygen doping via photo-Fenton reaction with enhanced photocatalytic activity, Appl. Catal. B-Environ. 185 (2016) 315–321.
[25] S. Guo, Z. Deng, M. Li, B. Jiang, C. Tian, Q. Pan, H. Fu, Phosphorus-Doped carbon nitride tubes with a layered micronanostructure for enhanced visible-Light photocatalytic hydrogen evolution, Angew. Chem. Int. Ed. 128 (2016) 1862–1866.
[26] Y. Kofuji, S. Ohkita, Y. Shiraishi, H. Sakamoto, S. Tanaka, S. Ichikawa, T. Hirai, Graphitic carbon nitride doped with biphenyl diimide: efficient photocatalyst for hydrogen peroxide production from water and molecular oxygen by sunlight, ACS Catal. 6 (2016) 7021–7029.
[27] P.-W. Chen, K. Li, Y.-X. Yu, W.-D. Zhang, Cobalt-doped graphitic carbon nitride photocatalysts with high activity for hydrogen evolution, Appl. Surf. Sci. 392 (2017) 608–615.
[28] M.Y. Ye, Z.H. Zhao, Z.F. Hu, L.Q. Liu, H.M. Ji, Z.R. Shen, T.Y. Ma, 0D/2D heterojunctions of vanadate quantum Dots/Graphitic carbon nitride nanosheets for enhanced visible-Light-Driven photocatalysis, Angew. Chem. Int. Ed. 129 (2017) 1–6.
[29] G. Liu, G. Zhao, W. Zhou, Y. Liu, H. Pang, H. Zhang, D. Hao, X. Meng, P. Li, T. Kako, J. Ye, In situ bond modulation of graphitic carbon nitride to construct p?n homojunctions for enhanced photocatalytic hydrogen production, Adv. Funct. Mater. 37 (2016) 6822–6829.
[30] J. Zhang, M. Zhang, R.Q. Sun, X. Wang, A facile band alignment of polymeric carbon nitride semiconductors to construct isotype heterojunctions, Angew. Chem. Int. Ed. 124 (2012) 10292–10296.
[31] Y. Chen, J.S. Zhang, M.W. Zhang, X.C. Wang, Molecular and textural engineering of conjugated carbon nitride catalysts for selective oxidation of alcohols with visible light, Chem. Sci. 4 (2013) 3244–3248.
[32] Z. Chen, P. Sun, B. Fan, Q. Liu, Z. Zhang, X. Fang, Textural and electronic structure engineering of carbon nitride via doping with –deficient aromatic pyridine ring for improving photocatalytic activity, Appl. Catal. B-Environ. 170–171 (2015) 10–16.
[33] J. Xu, L. Zhang, R. Shi, Y. Zhu, Chemical exfoliation of graphitic carbon nitride for efficient heterogeneous photocatalysis, J. Mater. Chem. A 1 (2013) 14766–14772.
[34] M. Zhang, X. Wang, Two dimensional conjugated polymers with enhanced optical absorption and charge separation for photocatalytic hydrogen evolution, Energ. Environ. Sci. 7 (2014) 1902–1906.
[35] J. Zhang, M. Zhang, S. Lin, X. Fu, X. Wang, Molecular doping of carbon nitride photocatalysts with tunable bandgap and enhanced activity, J. Catal. 310 (2014) 24–30.
[36] L. Ge, C. Han, J. Liu, Novel visible light-induced g-$C_3N_4$/$Bi_2WO_6$ composite photocatalysts for efficient degradation of methyl orange, Appl. Catal. B-Environ. 108–109 (2011) 100–107.
[37] Q. Xiang, J. Yu, M. Jaroniec, Preparation and enhanced visible-Light photocatalytic $H_2$-Production activity of Graphene/$C_3N_4$ composites, J. Phys. Chem. C 115 (2011) 7355–7363.
[38] J.S. Zhang, X. Chen, K. Takanabe, K. Maeda, K. Domen, J.D. Epping, X. Fu, M. Antonietti, X. Wang, Synthesis of a carbon nitride structure for visible-Light catalysis by copolymerization, Angew. Chem. Int. Ed. 122 (2010) 451–454.
[39] B. Chai, T. Peng, J. Mao, K. Li, L. Zan, Graphitic carbon nitride (g-$C_3N_4$)-Pt-$TiO_2$nanocomposite as an efficient photocatalyst for hydrogen production under visible light irradiation, Phys. Chem. Chem. Phys. 14 (2012) 16745–16752.

[40] J. Liu, Y. Liu, N. Liu, Y. Han, X. Zhang, H. Huang, Y. Lifshitz, S.T. Lee, J. Zhong, Z. Kang, Metal-free efficient photocatalyst for stable visible water splitting via a two-electron pathway, Science 347 (2015) 970–974.
[41] J.N. Qin, S.B. Wang, H. Ren, Y.D. Hou, X.C. Wang, Photocatalytic reduction of $CO_2$ by graphitic carbon nitride polymers derived from urea and barbituric acid, Appl. Catal. B-Environ. 179 (2015) 1–8.
[42] J.S. Zhang, X. Chen, K. Takanabe, K. Maeda, K. Domen, J.D. Epping, X. Fu, M. Antonietti, X. Wang, Synthesis of a carbon nitride structure for visible-Light catalysis by copolymerization, Angew. Chem. Int. Ed. 122 (2010) 451–454.
[43] B.V. Lotsch, M. Döblinger, J. Sehnert, L. Seyfarth, J. Senker, O. Oeckler, W. Schnick, Unmasking melon by a complementary approach employing electron diffraction, solid-State NMR spectroscopy, and theoretical calculations-Structural characterization of a carbon nitride polymer, Chem. Eur. J. 13 (2007) 4969–4980.
[44] B.Y. Peng, S.S. Zhang, S.Y. Yang, H.J. Wang, H. Yu, S.Q. Zhang, F. Peng, Synthesis and characterization of g-$C_3N_4$/$Cu_2O$ composite catalyst with enhanced photocatalytic activity under visible light irradiation, Mater. Res. Bull. 56 (2014) 19–24.
[45] Y. Cui, Z. Ding, P. Liu, M. Antonietti, X. Fu, X. Wang, Metal-free activation of $H_2O_2$ by g-$C_3N_4$ under visible light irradiation for the degradation of organic pollutants, Phys. Chem. Chem. Phys. 14 (2012) 1455–1462.